Inorganic Chemistry

Article

pubs.acs.org/IC

Influence of the co-Ligand on the Magnetic and Relaxation Properties of Layered Cobalt(II) Thiocyanato Coordination Polymers

Susanne Wöhlert,[†] Zbigniew Tomkowicz,[‡] Michał Rams,[‡] Stefan G. Ebbinghaus,[§] Lothar Fink,[∥] Martin U. Schmidt,[∥] and Christian Näther*,[†]

[†]Institut für Anorganische Chemie, Christian-Albrechts-Universität zu Kiel, Max-Eyth-Straße 2, 24118 Kiel, Germany

[‡]Institute of Physics, Jagiellonian University, 30-059 Krakow, ul. Reymonta 4, Poland

[§]Institut für Chemie, Martin-Luther-Universität Halle-Wittenberg, Kurt-Mothes-Str. 2, 06120 Halle Saale, Germany

[∥]Institut für Anorganische und Analytische Chemie, Johann Wolfgang Goethe Universität, Max-von-Laue-Str. 7, 60438 Frankfurt am Main, Germany

Supporting Information

ABSTRACT: Reaction of $Co(NCS)_2$ with 1,2-bis(4-pyridyl)-ethane (bpa) leads to the formation of $[Co(NCS)_2(bpa)_2]_n$, which, on heating, transforms into the new layered coordination polymer $[Co(NCS)_2(bpa)]_n$. This compound can also be prepared in solution, but because no reasonable single crystals are available, its crystal structure was determined from X-ray powder data from scratch. In the crystal structure of $[Co(NCS)_2(bpa)]_n$, the cobalt(II) cations are coordinated by two S-bonded and two N-bonded thiocyanato anions and two N atoms of the bpa co-ligands in a distorted octahedral geometry. The cobalt(II) cations are linked into chains by pairs of μ-1,3 bridging thiocyanato anions. These chains are further connected into layers by the 1,2-bis(4-pyridyl)-ethane ligand. The compound was magnetically characterized, and, for comparative purposes, the complementary magnetic study of a known and very similar compound, $[Co(NCS)_2(bpe)]_n$ (bpe = 1,2-bis(4-pyridyl)-ethylene), was also undertaken. The compounds differ in their interchain interactions, which are antiferromagnetic but significantly greater for $[Co(NCS)_2(bpe)]_n$. Magnetic measurements indicate that $[Co(NCS)_2(bpa)]_n$ is a canted antiferromagnet with Néel temperature T_N = 3.1 K and that $Co(NCS)_2(bpe)$ is an antiferromagnet with T_N = 4.0 K. Both compounds show a metamagnetic transition with a critical field $H_C \sim 40$ Oe and ~ 400 Oe, respectively. Magnetic relaxations were studied by means of dc and ac methods and analyzed using the Argand diagrams. Except for the thermally activated single chain and domain wall relaxations observed for both compounds, temperature-independent slow relaxations were observed for $[Co(NCS)_2(bpa)]_n$.

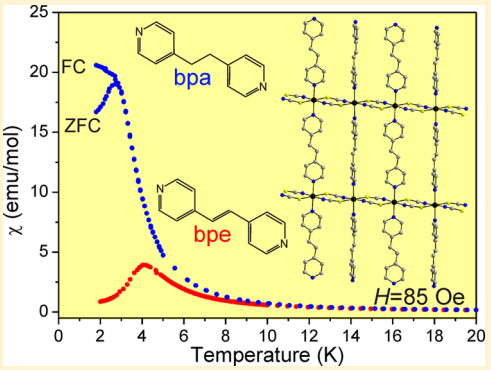

INTRODUCTION

Recently, the rational synthesis of new compounds that show a slow relaxation of magnetization, e.g., single-chain magnets (SCMs), has become of increasing interest.[1−10] For the preparation of such compounds, cations, which show a large uniaxial magnetic anisotropy, e.g., Co^{2+}, Mn^{3+}, and Fe^{2+}, have to be connected into chains with a high ratio of intrachain to interchain interactions.[1−3,10] In this context, several SCM compounds have been reported in the literature and investigated for their magnetic properties.[4,5,11−31]

In the past, we reported on a rational strategy for the preparation of chain and layered compounds based on transition metal thio- and selenocyanates.[32−37] Such compounds are less frequently reported in the literature, but they show interesting magnetic phenomena, especially if the anions act as bridging ligands.[38−48] We have found, e.g., that the compound $[Co(NCS)_2(pyridine)_2]_n$ showed a slow relaxation of magnetization, reminiscent of SCMs.[49] Further investigations revealed that the relaxations still exist if the anionic ligand is exchanged by selenocyanate, which leads to a significant increase in the intrachain interactions and the effective energy barrier for spin reversal.[50] During the course of this project, we also investigated corresponding Fe(II) compounds. The isotypic iron thiocyanato compound investigated by Foner et al. is a metamagnet that shows no relaxations, but if the anionic ligand is exchanged by selenocyanato anions, then the metamagnetic behavior is retained, and, in contrast to $[Fe(NCS)_2(pyridine)_2]_n$, a slow relaxation of magnetization is observed in $[Fe(NCSe)_2(pyridine)_2]_n$.[51,52] In this context, it is noted that the related compound $[Co(NCS)_2(4\text{-ethylpyridine})_2]_n$ also consists of thiocyanato chains, but in contrast to $[Co(NCS)_2(pyridine)_2]_n$, metamagnetic behavior is observed; thus, interchain interactions are not very small. Therefore, this compound is not an ideal SCM.[53] However, a similar magnetic behavior can also be observed in 2D coordination networks if

Received: March 14, 2014
Published: July 31, 2014

   dx.doi.org/10.1021/ic500572p | Inorg. Chem. 2014, 53, 8298−8310

the magnetic chains are separated by relatively large bridging ligands, and there are some examples that have been reported regarding this phenomenon.[22,54,55] Following these ideas, we exchanged the monodentate co-ligand pyridine by the bridging ligand *trans*-1,2-bis(4-pyridyl)-ethylene (bpe), which leads to the formation of a sample of composition $[Co(NCS)_2(bpe)]_n$, in which the cobalt(II) cations are linked by μ-1,3 bridging thiocyanato anions into chains that are further connected into layers by the co-ligands. Magnetic measurements reveal that metamagnetic behavior in this compound is observed with a slow relaxation of magnetization above and below the critical field H_c.[56] A similar behavior was also found for the selenocyanato analogue, which showed a significant increase of J_{intra}, H_c, and the effective energy barrier.[57] In this context, it is noted that the magnetic phase below H_c was not investigated in detail and that the energy barrier for the spin reversal was determined only from temperature-dependent ac measurements. A small exponent α of the generalized Debye mode, determined from these measurements, indicated a narrow distribution of the relaxation times and SCM behavior, but its temperature dependence was not investigated. However, the origin of the metamagnetic transition has still not been proven, but it is assumed that the ferromagnetic $Co(X)_2$ (X = NCS, NCSe) chains are antiferromagnetically coupled via the bpe ligand. If the magnetic field increases, then this coupling is overcome. This is also supported by our investigations on $[Fe(NCS)_2(bpe)]_n$, which also showed a metamagnetic transition.[58] All of these findings indicate that, despite the large interchain Co···Co distance of about 13.7 Å, the bpe ligand is involved in the magnetic exchange, which is reasonable because both pyridine rings are coplanar to the ethylene bridge, thus forming a conjugated π-system. To investigate the influence of the co-ligand in more detail, we decided to exchange *trans*-1,2-bis(4-pyridyl)-ethylene (bpe) by 1,2-bis(4-pyridyl)-ethane (bpa) (Scheme 1). In this case, the

Scheme 1. Structural Formula of 1,2-Bis(4-pyridyl)-ethylene (bpe) and 1,2-Bis(4-pyridyl)-ethane (bpa)

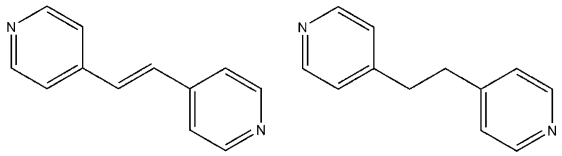

metamagnetic behavior might disappear or be suppressed, whereas the slow relaxation of magnetization might remain. In this context, it is noted that a compound of composition $[Co(NCS)_2(bpa)_2]_n$ has already been reported in the literature.[59−61] In its crystal structure, the metal centers are coordinated by two terminal N-bonded thiocyanato anions and four N-bonded bpa ligands and are linked into chains by the bpa co-ligands. Interestingly, thermogravimetric investigations show that half of the bpa ligands are removed on heating, which formally leads to a composition $[Co(NCS)_2(bpa)]_n$, exactly corresponding to the desired compound.[60] However, it was also reported in this work that this sample is of poor crystallinity and therefore no further investigations were performed at that time.

In this article, the structural as well as the static and dynamic magnetic properties of $[Co(NCS)_2(bpa)]_n$ are reported and are compared with those of $[Co(NCS)_2(bpe)]_n$ that were reported recently.[56] This also includes several new measurements on $[Co(NCS)_2(bpe)]_n$ that are needed for the comparison and which allow for more insight to be obtained into the magnetic properties of this compound. Attention is devoted to the relaxation properties both in the antiferromagnetic as well as in the field-induced phase.

RESULTS

Synthetic Aspects. Large amounts of the literature-known compound $[Co(NCS)_2(bpa)_2]_n$ can be easily prepared by the reaction of $Co(NCS)_2 \cdot H_2O$ with 1,2-bis(4-pyridyl)-ethane in water, and if the experimental X-ray powder pattern is compared with that calculated from literature data, then it can be seen that a phase-pure material is obtained (Figure S1, Supporting Information). As expected, IR spectroscopic investigations showed only one intense band for the asymmetric C−N stretching vibration at 2054 cm^{-1}, which is typical for terminal N-bonded thiocyanato anions (Figure S2, Supporting Information).

On heating, two mass steps are observed in the TG curve, which are accompanied by endothermic effects in the DTA curve (Figure S3, Supporting Information). The experimental mass loss Δm = 33.6% in the first TG step is in good agreement with that calculated for the removal of one bpa ligand (Δm = 33.8%). On further heating, the remaining bpa ligands are removed, and the cobalt thiocyanate formed as an intermediate decomposes. To verify the nature of the intermediate, an additional TG experiment was performed and stopped after the first TG step. The residue obtained was investigated by elemental analysis and IR spectroscopy, which showed that the composition exactly corresponds to $[Co(NCS)_2(bpa)]_n$ and that a value of 2103 cm^{-1} is observed for the C−N stretching vibration, which is expected if only μ-1,3 bridging thiocyanato anions are present (Figure S3, Supporting Information).[62,63] Further investigations prove that this compound can also be prepared in solution as a pure phase (Figure 1). Unfortunately,

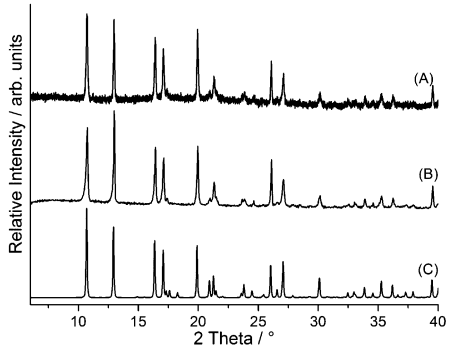

Figure 1. Experimental X-ray powder pattern of $[Co(NCS)_2(bpa)]_n$ prepared in solution (A) and by thermal decomposition of $[Co(NCS)_2(bpa)_2]_n$ (B) and powder pattern of $[Co(NCS)_2(bpa)]_n$ calculated from the crystallographic data obtained from the Rietveld refinement (C).

this compound is not isotypic to that with bpe, and all attempts to prepare single crystals suitable for single-crystal X-ray diffraction failed. Therefore, the structure was determined from X-ray powder data from scratch (Figure S4, Supporting Information).

Crystal Structure of $[Co(NCS)_2(bpa)]_n$. This compound crystallizes in the centrosymmetric space group $P2_1/n$, with Z =

dx.doi.org/10.1021/ic500572p | Inorg. Chem. 2014, 53, 8298−8310

4 formula units in the unit cell and all atoms in general positions. The crystal structure is very similar to that of the bpe analogue (see Figure S5, Supporting Information), but it is not isotypic. Each cobalt(II) cation is octahedrally coordinated by two N-bonded and two S-bonded thiocyanato anions as well as two N-bonded bpa ligands. The cobalt(II) cations are μ-1,3 bridged by pairs of thiocyanato anions into chains, which are further connected into layers by the bpa ligands (Figure 2).

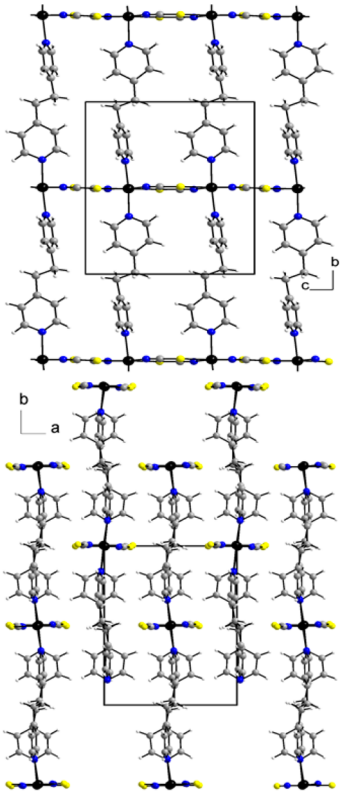

Figure 2. Crystal structure of $[Co(NCS)_2(bpa)]_n$: view of the layers from above (top) and along the cobalt thiocyanato chains (bottom).

In $[Co(NCS)_2(bpa)]_n$, the intrachain Co···Co distance along the thiocyanato chains amounts to 5.6113(3) Å, whereas the interchain Co···Co distance via the bpa coligand is 13.6812(3) Å. These values are comparable to those in $[Co(NCS)_2(bpe)]_n$ (intrachain Co···Co distance is 5.6482(10) Å; interchain Co···Co distance via the bpe coligand is 13.7157(13) Å). The layers are stacked with an interlayer Co···Co distance of 8.6692(3) Å, which is comparable to that in $[Co(NCS)_2(bpe)]$, 8.4184(8) Å.[56] In contrast to $[Co(NCS)_2(bpe)]_n$ in which the pyridine rings are coplanar, in $Co(NCS)_2(bpa)_n$, they are nearly perpendicular to each other. Therefore, they cannot be isotypic. Moreover, the $N_{Pyridine}-N_{Pyridine}$ vectors of chains belonging to neighboring columns in Figure 2 (bottom) are slightly canted, but because restraints were used in the Rietveld refinement, we cannot prove whether this is significant. It is noted that there is no canting of the $N_{Pyridine}-N_{Pyridine}$ vectors in the crystal structure of $[Co(NCS)_2(bpe)]_n$.

Magnetic and Relaxation Properties of $[Co(NCS)_2(bpa)]_n$. *Static and Quasi-Static Magnetic Properties.* The magnetic susceptibility χ of $[Co(NCS)_2(bpa)]_n$ was measured as a function of temperature in the temperature range $2.0 \leq T \leq 300$ K and in a magnetic field of 100 Oe. The experimental data are shown in the Figure 3 (below 150 K),

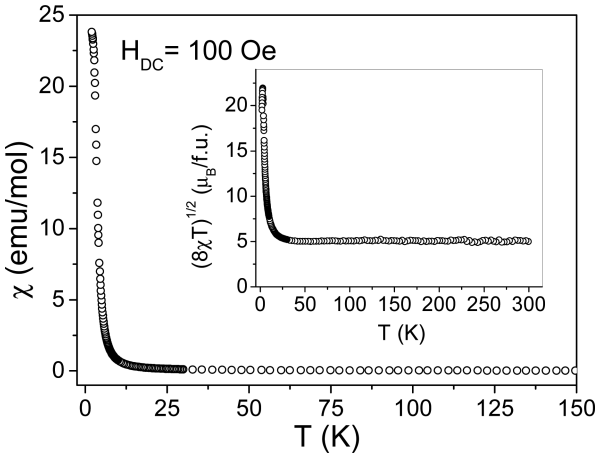

Figure 3. Temperature dependence of the magnetic susceptibility of $[Co(NCS)_2(bpa)]_n$ measured during cooling in a field of 100 Oe. The inset shows the temperature dependence of the effective magnetic moment.

and the inset of Figure 3 shows the temperature dependence of the effective magnetic moment $\mu_{eff} = (8\chi T)^{1/2}$. As follows from these data, $\chi(T)$ is a slowly increasing function with decreasing temperature, but at the lowest temperatures, it strongly increases and shows some degree of saturation. Also, the $\mu_{eff}(T)$ value, which is nearly constant at higher temperatures, shows a strong increase on cooling (below ~25 K), indicating a dominant ferromagnetic coupling. However, below 2.9 K, it slightly decreases. The high-temperature value of μ_{eff} equals $5.16 \pm 0.05\mu_B$ and is considerably greater than the spin-only value of $3.87\mu_B$ expected for $s = {}^3/_2$, pointing to the orbital contribution. This nearly constant value of μ_{eff} above ~40 K is a result of an accidental compensation of the spin−orbit[64] and magnetic coupling effects.

To obtain insight into the intrachain exchange interaction J, we initially used the $\ln(\chi T)$ vs reciprocal temperature dependence (Figure S6, Supporting Information). The linear part of this dependence is characteristic for a 1 D anisotropic system, and its slope, $\Delta\xi/k_B = 12.2$ K, equals the energy of the creation of a domain wall.[10] From the relation $\Delta\xi = 2s^2J$ (assuming $s = {}^1/_2$), a value of $J/k_B \sim 24$ K is obtained. More information, however, may be obtained by fitting a theoretical model to the data acquired in very low magnetic field. To this end, we used ac magnetic susceptibility data (Figure 4).

For a strongly anisotropic chain system of Co(II) ions in an axially distorted octahedral coordination, the following Ising Hamiltonian with spin $s = {}^1/_2$ is adequate at low temperatures.[64]

$$\mathcal{H} = \sum_i \{-Js_i^z s_{i+1}^z + \mu_B H\cdot\hat{g}\cdot s_i\} \quad (1)$$

where J is the intrachain exchange interaction. The expressions for the parallel and perpendicular susceptibility derived from this Hamiltonian (for $H \sim 0$) by Fisher[65] are

$$\chi_{\parallel} = \frac{N_A\mu_B{}^2 g_{\parallel}{}^2}{4kT}\exp(K) \quad (2)$$

$$\chi_{\perp} = \frac{N_A\mu_B{}^2 g_{\perp}{}^2}{2J}\{\tanh(K/2) + K/[2\cosh^2(K/2)]\} \quad (3)$$

dx.doi.org/10.1021/ic500572p | Inorg. Chem. 2014, 53, 8298−8310

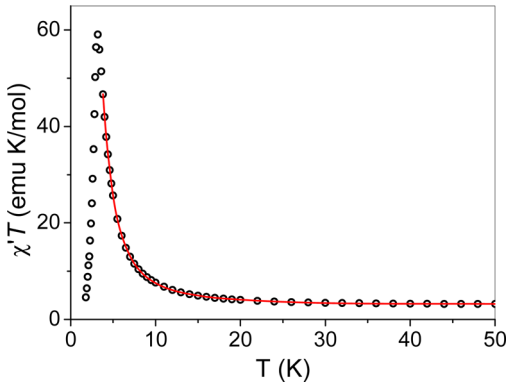

Figure 4. Temperature dependence of the $\chi'T$ product for $[Co(NCS)_2(bpa)]_n$. χ' is the in-phase component of the molar ac susceptibility measured in a zero dc bias magnetic field at 10 Hz frequency and by the amplitude of the driving magnetic field of 3 Oe. The solid line is a fit according to the Ising chain model (see text).

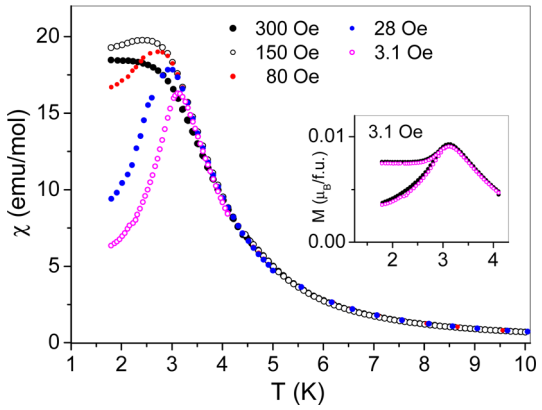

Figure 5. Temperature dependence of the magnetic susceptibility of $[Co(NCS)_2(bpa)]_n$ measured in a ZFC regime plotted for five different magnetic field strengths. The inset shows ZFC and FC data for 3.1 Oe. For this field, the data were obtained with different rates of the field change (see text), but they overlap perfectly.

where $K = J/(2k_BT)$ and $g_\parallel$ and $g_\perp$ are g factors defined for the magnetic field directed parallel and perpendicular to the easy direction of anisotropy, respectively. The final equation for the powder-averaged susceptibility of our system of weakly interacting chains is derived on the basis of the mean field approximation

$$\chi = \chi_{chain} \Big/ \left(1 - \frac{zJ'}{N_A g^2 \mu_B{}^2}\chi_{chain}\right) \quad (4)$$

where χ_{chain} is the susceptibility of noninteracting chains and zJ' is the interchain interaction. Thus, the The expression for the χT product, thus obtained, was fitted to the experimental curve shown in Figure 4. The best fit parameters are $J/k_B = 28.1 \pm 0.5$ K, $g_\parallel = 7.64 \pm 0.05$, $g_\perp = 1.05 \pm 0.50$, and $zJ'/k_B = -0.22 \pm 0.05$ K. This gives quite a small value for the $|zJ'/J|$ ratio of $\sim 8 \times 10^{-3}$. It is noted that the value for the intrachain interaction of 28.1 K is in reasonable agreement with that obtained from the slope of the $\ln(\chi T)$ vs $1/T$ curve ($J/k_B \sim 24$ K). Instead, the $|zJ'|$ value may not be exactly determined because only one average value can be found for a powder sample. This value may be also influenced by the demagnetization effect and canting of anisotropy axes. Because $zJ' < 0$, the ground magnetic state of this compound may be antiferromagnetic. In such a case, a metamagnetic transition is expected to occur in some critical field.

In the next step, temperature-dependent magnetization measurements were performed under FC/ZFC conditions (see Experimental Section). Depending on whether these data were registered in a ZFC or FC regime, a bifurcation of $\chi(T)$ curves at low temperatures was observed (Figure 5, inset, and Figure S7, Supporting Information). In Figure 5, only ZFC curves are shown. It is seen that sharp maximum, observed for 30 Oe fields, disappears with increasing field but still exists in 150 Oe. It also shows a small bifurcation, which is even seen in 300 Oe (Figure S7). On the basis of these data, it may be concluded that the saturated paramagnetic phase is met just above 300 Oe, but somewhere between 30 and 150 Oe a metamagnetic transition occurs. It is noted that the maximum of $\chi(T)$ falls at 3.1 K (in the lowest field of 3.1 Oe; see inset to Figure 5) and moves to lower temperature with increasing field, as expected for an antiferromagnet.

The data for 3.1 Oe were obtained with two different rates of the field change, 0.2 and 0.05 K/min. They nearly perfectly overlap in the figure. No relaxation of magnetization toward FC data during measurement was observed, which means that the relaxation time is at least 20 min. Additionally, the maximum of the curve, being independent of the field rate change, indicates that the transition is not to a spin glass state.[66] This overall behavior is consistent with canted antiferromagnetism and domains present due to an uncompensated magnetic moment. This can be understood with the help of Figure 2 (bottom panel) by assuming no coupling along the bpa ligand but antiferromagnetic, through space (dipolar), coupling between chains of neighboring columns.

Isothermal field-dependent magnetization data obtained at 1.8 K are presented in Figure 6; the data for other temperatures

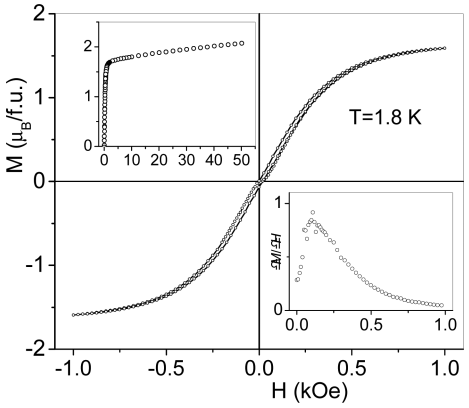

Figure 6. Hysteresis loop for $[Co(NCS)_2(bpa)]_n$ recorded at 1.8 K. The upper inset shows $M(H)$ measured at 1.8 K up to 50 kOe. The lower right inset shows the derivative $\partial M/\partial H$ of the virgin curve (in arbitrary units).

in the limited field range −500 to 500 Oe are shown in Figure S8, Supporting Information. The observed hysteresis loop is very narrow, and, in addition, it shows a constriction near $H \sim 0$ Oe. With increasing temperature, the loop narrows, and at 2.5 K, it collapses in the middle before closing completely.

The virgin curve was differentiated, and the resulting $\partial M/\partial H$ curve is plotted in the bottom inset of Figure 6; see also Figure S9, Supporting Information. The occurrence of a maximum at 110 Oe may be a sign of a metamagnetic transition. It might be associated with a flip of the magnetic moment of some chains in

dx.doi.org/10.1021/ic500572p | Inorg. Chem. 2014, 53, 8298−8310

the canted magnetic structure to a more favorable, with respect to the field, direction. The magnetization curve measured in the large field range up to 50 kOe is shown in the upper inset of Figure 6. It is noted that even at 50 kOe no saturation is observed, which is in accordance with the high anisotropy of Co(II) ions and with a canting of magnetic moments.

As mentioned above, the bifurcations observed in the FC/ZFC measurements (Figure 5 inset) are a manifestation of a slow relaxation process. In order to estimate the mean relaxation time τ, the time dependence of magnetization was measured according to the following procedure, which was repeated for several different temperatures. In the beginning, the temperature was set at 5 K, and the sample was then cooled in zero field to a specified temperature. After waiting, which was needed to ensure a good temperature stabilization, the field of 30 Oe was switched on, and the measurement started. The data obtained were fitted according to the stretched exponential function

$$M = M_0 + \Delta M e^{-(t/\tau)^{1-n}} \quad (5)$$

The experimental data and fits are shown in Figure 7 (for the data on the linear scale, see Figure S10, Supporting Information). The relaxation times obtained from fits are ~1070 ± 30 s, practically independent of temperature. The n parameter ($0 \leq n \leq 1$) describes a distribution of energy barriers (a single barrier, as expected for perfect SCM, would correspond to $n = 0$). The n value obtained from all fits is 0.68 ± 0.05, which shows that this distribution is broad. It is noted that the M_0 value is not equal to zero and increases with increasing temperature. It points to another relaxation process, which takes place immediately after switching the field on. Also, ΔM is not constant: it slightly decreases with increasing temperature. The obtained relaxation time is lower than that deduced from the FC/ZFC data in a field of 3.1 Oe (see inset to Figure 5), which is understandable when taking into account the fact that a higher field of 30 Oe was now being used and that the relaxation time should decrease with increasing field. It is noted that the relaxation time measured for the sample cooled in field of 100 Oe after switching the field off was only ~360 s (see Figure S11, Supporting Information); however, it was long enough to observe the bifurcations in that field and in higher fields; see Figure 5.

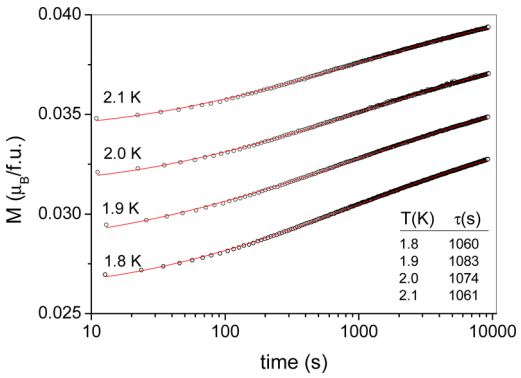

Figure 7. Time-dependent magnetization measured for a zero-field cooled sample of $[Co(NCS)_2(bpa)]_n$ after switching on a field of 30 Oe. Solid lines are fits. The table shows relaxation times τ obtained from fits for various temperatures.

ac Properties. For further study of the relaxation properties of $[Co(NCS)_2(bpa)]_n$, we used the standard ac susceptibility method. Figure 8 presents ac susceptibility data ($\chi = \chi' - i\chi''$ in complex notation) obtained as a function of temperature for various frequencies in two different bias magnetic fields. Zero field is to probe the ground state, and the 100 Oe field is to probe the mixed phase, which appears above the critical field. In Figure S12, measurements at higher fields are presented, which were performed to suppress the domain walls response in order to see possible SCM relaxations.

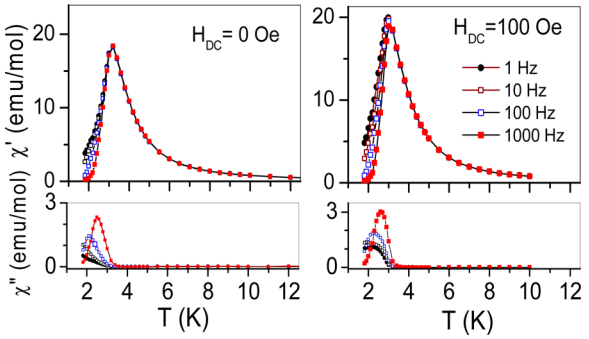

Figure 8. Temperature-dependent ac susceptibility of a $[Co(NCS)_2(bpa)]_n$ sample measured for various frequencies in two different dc bias magnetic fields. The legend applied to the whole figure.

In zero dc field, the in-phase component χ' shows a maximum at T_N = 3.15 K, which does not shift with frequency and which should correspond to the antiferromagnetic transition. Such behavior confirms that this maximum is the manifestation of a phase transition, excluding superparamagnetic blocking, which is observed when, with decreasing temperature, the relaxation time becomes so long that the system is not able to respond during the measurement time.[67] The frequency dispersion of χ' and the out-of-phase component χ'' are centered to the left of the χ' maximum; however, the tail of the χ'' peak exceeds T_N, and for the highest available frequency of 10 000 Hz, it extends above 4 K (not shown in the figure). In addition, the intensity of the χ'' peak increases with increasing frequency, which is in contrast with the behavior of an ideal SCM[68] but is consistent with SCM relaxations in the antiferromagnetic phase, see, e.g., ref 69. It is noted that the $\chi'(T)$ curve at zero frequency limit corresponds to the $\chi_{dc}(T)$ curve recorded in the ZFC regime, as seen in Figure S13, Supporting Information. At 100 Oe, the χ' maximum is shifted to lower temperatures (3.0 K). The frequency dispersion of χ' in this field is observed in a more extended temperature range, including the maximum position. Above 100 Oe, the χ' maximum moves to higher temperatures with increasing field and is frequency independent, as observed for 1000 Oe (see Figure S12).

It can be also seen in Figure 8 (and S12) that the heights of both the χ' and χ'' maxima depend on the dc bias field. This is better seen in Figure 9, which presents the bias field dependence of ac susceptibility. There is a clear maximum of χ_{ac} at 175 Oe, the occurrence of which is consistent with the metamagnetic transition to the mixed phase consisting of ferro- and antiferromagnetic domains, similar to that found in $[Co(NCS)_2(4\text{-ethylpyridine})_2]_n$, another compound in this family.[53] The critical field of the metamagnetic transition may be roughly determined from the maximum of the field

dx.doi.org/10.1021/ic500572p | Inorg. Chem. 2014, 53, 8298−8310

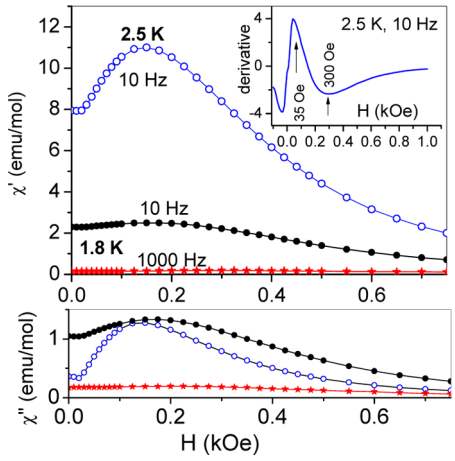

Figure 9. ac susceptibility of $[Co(NCS)_2(bpa)]_n$ as a function of bias dc magnetic field recorded for two different temperatures and two frequencies. The inset shows the derivative $\partial\chi'/\partial H$, of which two extremes are shown by arrows.

derivative of χ' and is equal to ~35 Oe at 2.5 K (see inset to Figure 9) and to ~40 Oe at 1.8 K. The $\chi_{ac}(H)$ dependence in the paramagnetic phase is shown in Figure S14.

From the $\chi''(T)$ data obtained in 5 Oe, the Mydosh parameter $\varphi = (\Delta T_p/T_p)/\Delta(\log f)$ was calculated to be 0.11 (T_p is the peak temperature of χ''). This value is in the range of values typical for superparamagnets or SCMs but is above the values expected for spin glasses.

To further explore the spin dynamics of $[Co(NCS)_2(bpa)]_n$, the ac susceptibility was measured as a function of frequency at various temperatures for several bias dc fields: 5, 175, 500, 1000, and 2000 Oe. The data, obtained in the bias field of 5 Oe, are shown in Figure 10, and the data obtained in zero field in another frequency and temperature range are shown in Figure S15. Data for 175 and 1000 Oe are shown in Figures S16 and S17, respectively.

All of these data were fitted with the generalized Debye model, in which the possible presence of two relaxation processes was allowed

$$\chi = \chi' - i\chi'' = \chi_\infty + \left\{ \frac{\delta_1}{1 + (i\omega\tau_1)^{1-\alpha_1}} + \frac{\delta_2}{1 + (i\omega\tau_2)^{1-\alpha_2}} \right\} \quad (6)$$

where $\delta_1 = \chi_0 - \chi_{\infty 1}$ and $\delta_2 = \chi_{02} - \chi_\infty$ may be called (by analogy to dielectric spectroscopy) magnetic intensity or magnetic increment, χ_0 and χ_∞ are susceptibilities in the limit of zero and infinite frequency, respectively, τ_1 and τ_2 are the relaxation times, and α_1 and α_2 are parameters related with the widths of the relaxation times distributions ($0 \le \alpha \le 1$). $\alpha = 0$ corresponds to a unique relaxation time, as expected for ideal SCM's, and $\alpha \to 1$ corresponds to an infinity of relaxation times. We put $\chi_{02} = \chi_{\infty 1}$. Good fits with a single distribution of relaxation times were obtained for $H_{dc} = 5$ Oe above 2.8 K and for 2000 Oe in the whole studied temperature range, 2.0–3.4 K. For 1000 Oe, a trace of a slow process appears at about 2.8 K but is not observed at lower temperatures because of the limited frequency range. The rest of data could not be fitted with a single distribution; however, relatively good fits were obtained with two distributions except for the data at 500 Oe, where the quality of the fit was poor. The best fit parameters for the 0 Oe field (two distributions below $T = 2.5$ K) and for the

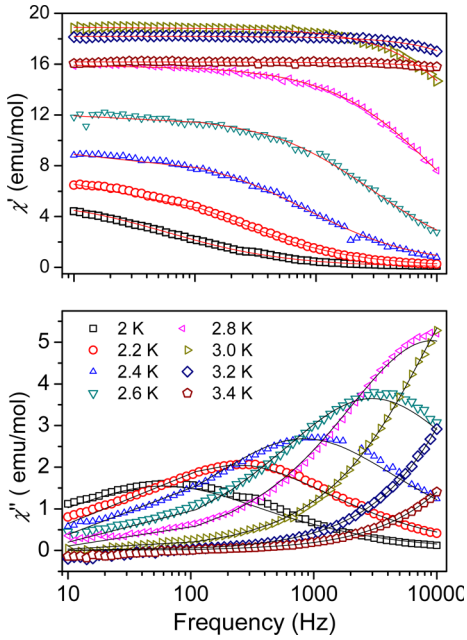

Figure 10. ac susceptibility of $[Co(NCS)_2(bpa)]_n$ measured as a function of frequency at various temperatures for 5 Oe dc bias field. Solid lines are fits.

1000 Oe field (one distribution) are shown in Tables S1 and S2, respectively, in the Supporting Information. The highest value of the relaxation time obtained from all fits was ~0.2 s (at 1.8 K).

Using the parameters obtained from fits, one may illustrate the component processes by means of their arcs in Argand diagrams; see Figures 11 and S18–S22. The diagrams for a bias

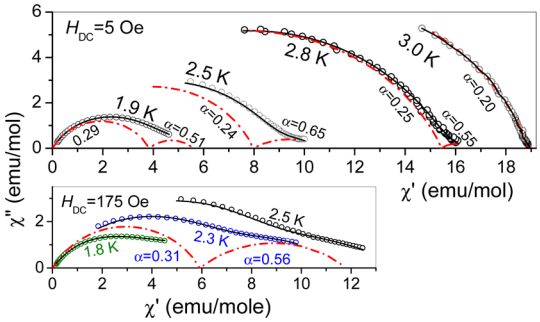

Figure 11. Argand diagrams for $Co(NCS)_2(bpa)$ in dc fields of 5 and 175 Oe at several temperatures. Solid lines are fits. The arcs of component processes are shown as red dot–dashed lines.

field of 5 Oe and for the temperature range 3.4–3.0 K (i.e., above and in the vicinity of the critical temperature, 3.1 K) show a single process with the corresponding α parameter increasing with decreasing temperature from 0.12 at 3.4 K to 0.20 at 3.0 K. At 2.8 K, a small contribution from a second, slow process with $\alpha = 0.55$ appears in the Argand diagram. It is clearly seen at the highest values of χ' (~16 emu/mol). The intensity of this process is three times greater at 2.6 K. At 2.5 K, a flattening of the χ'' vs χ' curve appears (also see Figure S19). The calculated relaxation time τ for the slow process at this temperature is ~9 ms. However, it should be taken into account that the χ_0 parameter cannot be well-estimated because of this flattening. By fixing a greater value of χ_0, a greater value

dx.doi.org/10.1021/ic500572p | Inorg. Chem. 2014, 53, 8298–8310

of τ may be obtained with a comparable quality of the fit. With decreasing temperature, the flattening is no longer visible because of the limited low frequency range. The greatest relaxation time at the lowest temperature range may be much greater than that from the decomposition of two arcs of the observed relaxation spectrum (τ value corresponding to the arc with α = 0.51 at 1.9 K is 0.13 s).

The slower process, which appears in the bias field of 5 Oe below T_N, has a large value of α. It is believed that this process is related with domain wall relaxations. These domains appear because of uncompensated moment due to canting. The faster process, which was extracted directly below T_N, seems to follow the relaxation process above T_N. It may be the SCM process. Its α value, ~0.25, is in range of values reported in the literature for SCM systems; see, e.g., refs 2 and 55. The relaxation time of this process showed thermal activation in accordance with the Arrhenius relation

$$\tau = \tau_0 e^{\Delta_\tau / kT} \quad (7)$$

The reciprocal temperature dependence of $\ln(\tau)$ is plotted in Figure 12. The energy barrier obtained from the fit with eq 7 is 39.2 K. The corresponding prefactor τ_0 is 1.2×10^{-11} s.

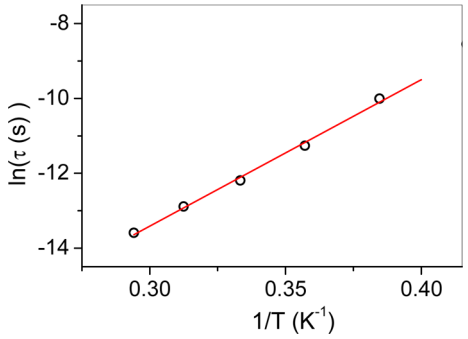

Figure 12. Logarithm of relaxation time vs reciprocal temperature for $Co(NCS)_2(bpa)$ in a dc bias field of 5 Oe. Solid line is a linear fit.

In a field of 175 Oe, the sample is in the mixed phase, composed of antiferromagnetic domains with a weak uncompensated magnetic moment and ferromagnetically field-aligned domains with a greater magnetic moment. The magnetization reversal in response to an ac field is due to moving walls between these domains. The corresponding Argand diagrams are presented at the bottom of Figure 11. It was not possible to differentiate any process with a linear $\ln(\tau)$ vs $1/T$ dependence.

The $\ln(\tau)$ vs $1/T$ plots for higher bias fields, 1000 and 2000 Oe, are given in Figure S23, Supporting Information. The barrier height for 500 Oe could not be reliably determined. The heights of barrier in fields 5, 1000, and 2000 Oe are given in Table 1. As seen, barrier heights are clearly lower in fields of 1000 and 2000 Oe. The α value in a field of 2000 Oe varies from 0.12 at 3.4 K up to 0.41 at 2.0 K.

Magnetic and Relaxation Properties of $[Co(NCS)_2(bpe)]_n$: Comparative Study. To investigate the influence of ligand exchange, the magnetic properties of $[Co(NCS)_2(bpa)]_n$ were compared with those of $[Co(NCS)_2(bpe)]_n$. Preliminary results for $[Co(NCS)_2(bpe)]_n$ have already been published,[56] but detailed measurements were lacking. It is noted that $Co(NCS)_2(bpe)$ is a metamagnet with a critical field of $H_c \sim 400$ Oe. In Figure 13, the temperature dependence of the molar susceptibility of this compound measured in a dc field of 100 Oe is shown. The peak temperature read from the inset is 4.0 K.

Table 1. Selected Experimental Results of the Magnetic Investigations[a]

	$[Co(NCS)_2(bpa)]_n$	$[Co(NCS)_2(bpe)]_n$
T_N (K)	3.1 ± 0.1	4.04 ± 0.1
H_c (Oe; at 2 K)	~40	~400
J/k_B (K)	+28.1 ± 0.5	+25.9 ± 0.4
zJ'/k_B (K)	−0.22 ± 0.05	−0.76 ± 0.04
Δ_τ/k_B (K); τ_0 (5 Oe)	39.2 ± 1.4; (1.2 ± 0.6) × 10^{-11}	33.3 ± 1.0; 1.2 × 10^{-11}
Δ_τ/k_B (K); τ_0(500 Oe)		42.7 ± 2.2; 1.2 × 10^{-11c}
Δ_τ/k_B(K); τ_0 (1000 Oe)	35.9 ± 1.0; 3.7 × 10^{-11}	42.1 ± 1.5; 1.8 × 10^{-11c}
Δ_τ/k_B(K); τ_0 (2000 Oe)	33.4 ± 1.0; 7.7 × 10^{-11}	42.0 ± 1.5; 1.1 × 10^{-11c}
α^b	0.06−0.41	0.10−0.46

[a] τ_0 is given in seconds. [b] Limit values; they depend on field and temperature. [c] Values for the single-barrier domain process (see text).

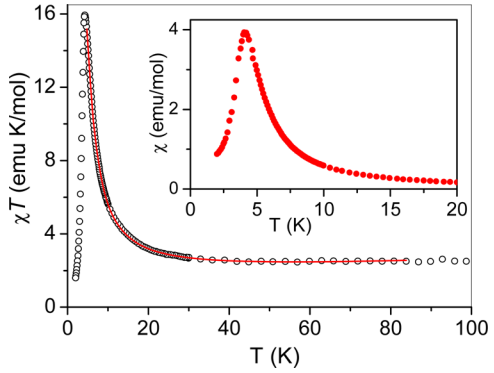

Figure 13. Temperature dependence of χT product for $[Co(NCS)_2(bpe)]_n$. χ is dc susceptibility, for which temperature dependence is separately shown in the inset. Measurement was done in a dc field of 100 Oe for the sample cooled in this field. The solid line is a fit according to the Ising chain model (see text).

The parameters obtained by fitting the Ising chain model, as described above, are J = +25.9 ± 0.4 K, zJ' = −0.76 ± 0.04 K, $g_\parallel$ = 7.34 ± 0.04, and $g_\perp$ = 0 ± 0.04. The value of J is very similar to that obtained for $[Co(NCS)_2(bpa)]_n$, which is reasonable because the same cobalt thiocyanato chains are found in both compounds. The ratio of the interchain to intrachain interactions ($|zJ'/J| = 0.76/25.9 > 3 \times 10^{-2}$) is nearly four times greater than that for $[Co(NCS)_2(bpa)]_n$, which shows that bpe mediates interchain interactions.

FC vs ZFC measurements of the magnetic susceptibility were performed in various magnetic fields (Figure 14). In contrast with $[Co(NCS)_2(bpa)]_n$, no bifurcations were observed between 50 and 1000 Oe. Magnetization measurements as a function of field were already presented in the previous study, and no $M(H)$ hysteresis was observed.[56]

The dc bias field dependence of the ac magnetic susceptibility was measured at three temperatures at a frequency of 10 Hz (Figure 15). The maximum, seen for a field of 590 Oe, is related with domain wall relaxations in the mixed phase, which appears to be due to the metamagnetic

dx.doi.org/10.1021/ic500572p | Inorg. Chem. 2014, 53, 8298−8310

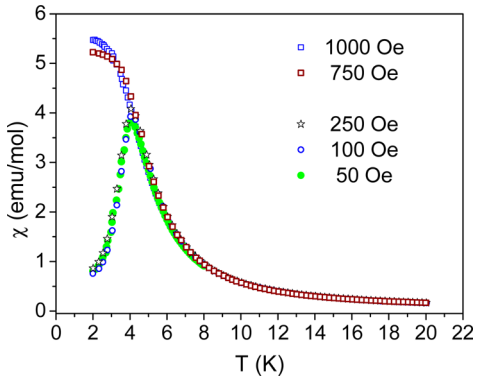

Figure 14. Temperature dependence of the dc magnetic susceptibility for $[Co(NCS)_2(bpe)]_n$ measured in various fields. All measurements were done both in FC and ZFC regimes, but no bifurcations were observed (data for 750 and 1000 Oe, corresponding to $H > H_c$, show no maximum).

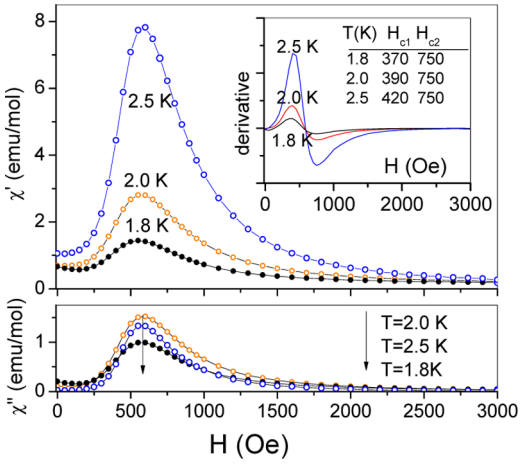

Figure 15. Field-dependent ac susceptibility of $Co(NCS)_2(bpe)$ measured at three temperatures with an amplitude of the ac driving field of 3 Oe and a frequency of 10 Hz. The inset shows the derivative $\partial\chi'/\partial H$, the extremes of which (at H_{c1} and H_{c2}) approximately determine the borders of the mixed phase.

transition. It is worth noting that the values of χ'' for H close to zero are much smaller than the value at the maximum.

This differs from the behavior observed for $[Co(NCS)_2(bpa)]_n$ (compare with Figure 9) and is consistent with the conclusion on domain relaxation in $[Co(NCS)_2(bpa)]_n$ at low temperatures in a field of 5 Oe. The extremes of the field derivative of χ' (see inset to Figure 15) roughly determine the borders of the mixed phase. They will be used later to construct an approximate phase diagram. We would like to note that the H_C value obtained from the previously published $M(H)$ curve (for T = 2.0 K) by extrapolation of the linear part of this curve in the field range just above H_C, to the intersection with M = 0 line is 395 ± 5 Oe in the nice agreement with the value of 390 Oe obtained from the present ac data.

The temperature-dependent ac susceptibility of $[Co(NCS)_2(bpe)]_n$ was measured for various frequencies and in various dc bias magnetic fields. Figure 16 presents data obtained for two fields: 5 and 500 Oe. The maximum, observed for 5 Oe, manifests a phase transition to the antiferromagnetic state at the Néel point T_N = 4.2 K (4.0 K in a dc field of 100 Oe). The χ' dispersion is observed at low

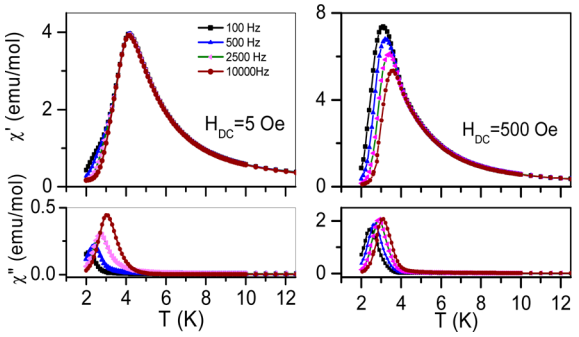

Figure 16. Temperature-dependent ac susceptibility measured for $[Co(NCS)_2(bpe)]_n$ at various frequencies in two bias dc magnetic fields.

temperatures in a field of 5 Oe, but in higher fields (above critical one ~400 Oe), it extends to higher temperatures. This behavior is similar to that for the bpa compound; however, the increase of susceptibility at the metamagnetic transition is much more remarkable (consistent with Figure 15).

To gain information on the relaxation times, the isothermal, frequency-dependent susceptibility was measured at various temperatures between 2.0 and 3.4 K in bias dc magnetic fields of 5, 500, 1000, and 2000 Oe (experimental data are shown in Figures S26–S29, Supporting Information). These data were fitted with the generalized Debye model as described above. The best fit parameters for bias fields of 5 and 500 Oe are given in Tables S3–S4, Supporting Information. The data for a bias field of 5 Oe could be well-fitted with one distribution of relaxation times. In contrast, for 500 and 1000 Oe, a reasonable agreement could be achieved by assumption of two distributions of relaxation times. Even for 2000 Oe, a small intensity of a second, slow process is seen; also see Figure S30. The corresponding Argand diagrams for fields of 5 and 500 Oe are shown in Figure 17.

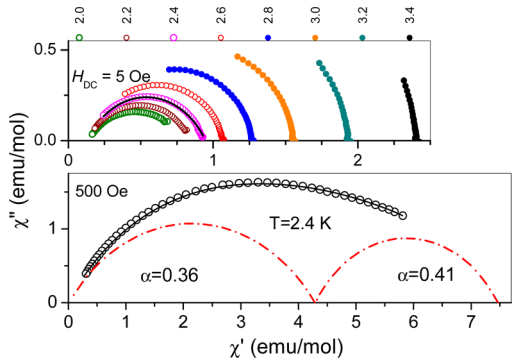

Figure 17. Argand diagrams for $[Co(NCS)_2(bpe)]_n$ in a field of 5 Oe for various temperatures (top panel) and for a field of 500 Oe for 2.4 K (bottom panel). Solid lines are fits (in the top panel, fit is shown only for 2.4 K). The arcs of extracted processes are plotted with the dot–dashed red line. The row of numbers at the top contains temperatures for particular arcs.

The χ'' vs χ' curves are ideal arcs for a field of 5 Oe and are consistent with the existence of only one (SCM) process. Its α value increases with decreasing temperature from 0.10 to 0.46 (see Table S3). The Argand diagrams for 500 Oe show distorted arcs, which can be decomposed into two arcs corresponding to different processes, possibly both related

dx.doi.org/10.1021/ic500572p | Inorg. Chem. 2014, 53, 8298–8310

with domain wall relaxations. The faster process cannot be resolved at the lowest temperature of 2.0 K (see Figure S30 and Table S4, Supporting Information) because the frequency band is too narrow. Argand diagrams for other temperatures in a field of 500 Oe and fields of 1000 and 2000 Oe are shown in Figures S30–S32.

On the basis of the fitting results of the $\chi_{ac}(f)$ curves, it was found that for all bias fields the faster process showed single-barrier thermal activation. The graphs presenting $\ln(\tau)$ vs $1/T$ dependence for different bias fields are shown in Figure 18 (the graph for 2000 Oe was omitted to prevent the figure from being obscured). The parameters in the Arrhenius relation ΔE and τ_0, which were obtained from fits, are given in Table 1. As seen, ΔE increases by entering the mixed phase.

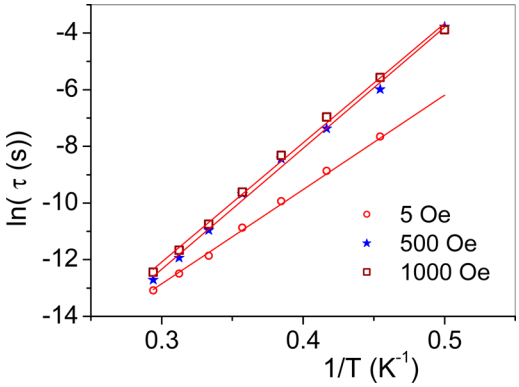

Figure 18. Logarithm of the relaxation time vs reciprocal temperature of $[Co(NCS)_2(bpe)]_n$ for three different bias magnetic fields.

DISCUSSION

Comparative studies of the magnetic properties of two coordination polymers, $[Co(NCS)_2(bpa)]_n$ and $[Co(NCS)_2(bpe)]_n$, have been carried out. These compounds are not isotypic, but their crystallographic structures are very similar, with one essential difference: the central double bond in bpe is exchanged by a single bond in bpa. It was expected that because of the π-conjugated system 1,2-bis(4-pyridyl)-ethylene would be more effective at transferring the interchain magnetic interaction and that the metamagnetic transition observed in $[Co(NCS)_2(bpe)]_n$ might therefore be suppressed in $[Co(NCS)_2(bpa)]_n$. However, both compounds are antiferromagnets (the compound with bpa is a canted antiferromagnet), and both exhibit the metamagnetic transition. We confirmed that this interchain interaction (zJ') is several times greater for $[Co(NCS)_2(bpe)]_n$. Accordingly, the critical field for the metamagnetic transition is also several times greater for this compound. We conclude that the interchain interaction through the bpa ligand in $[Co(NCS)_2(bpa)]_n$ is practically switched off and that the effective interchain interactions in this compound are dipolar interactions. All magnetic parameters extracted from fits for both compounds are collected in Table 1.

From measurements presented above, the magnetic phase diagram in the H–T plane was constructed for both compounds, each based on the external field Ha (Figure 19). In this case, the diagram consists of three different magnetic phases (CAF, canted antiferromagnetic phase; AF, antiferromagnetic phase; M, mixed phase; and P, saturated paramagnetic phase). The low-temperature points (1.8–2.5 K) in the two borderlines of the mixed phase were roughly obtained from ac data shown in Figures 9 and 15, taking extremes of $\partial\chi'/\partial H$ (but not extrapolating to f = 0 Hz).[70–73] The high-temperature points were obtained both from dc data (such as in Figures 5, S13, and S14) as well as from ac data (such as in Figure S12).

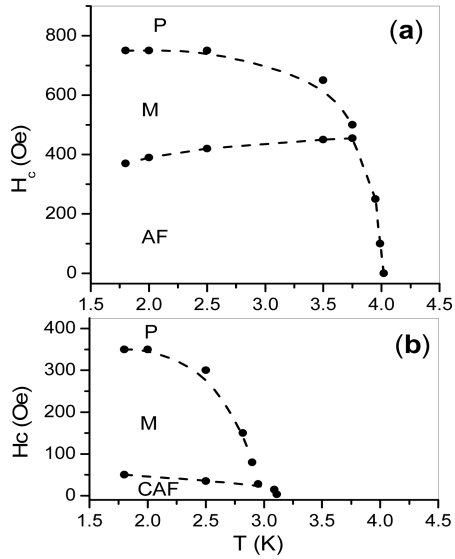

Figure 19. Phase diagram for powder samples of $[Co(NCS)_2(bpe)]_n$ (a) and $[Co(NCS)_2(bpa)]_n$ (b). AF, antiferromagnetic phase; CAF, canted antiferromagnetic phase; M, mixed phase; and P, saturated paramagnetic phase. Dashed lines are only a guide for the eye.

It was shown that both compounds demonstrate magnetic relaxations. For $[Co(NCS)_2(bpa)]_n$, the relaxation spectrum, obtained with ac method in a ~0 Oe dc bias field near T_N = 3.1 K and above, may be described with one process, likely related with SCM relaxations. At lower temperatures, an additional relaxation process appears, which is related with domain walls. Domains are present because of an uncompensated magnetic moment in the canted antiferromagnetic structure. In the applied field of ~40 Oe, the canted antiferromagnetic phase changes to another phase, which is the canted ferromagnetic phase mixed with the saturated paramagnetic phase. In this intermediary phase, only the domain wall relaxations are observed for $[Co(NCS)_2(bpa)]_n$ because they dominate the magnetic response.

dc magnetometry supplies additional information. The relaxation time τ of $[Co(NCS)_2(bpa)]_n$ in low dc bias fields and at low temperatures of ~2 K is much longer than observed by the ac method, so FC/ZFC bifurcations and the hysteresis appear. The value of τ does not depend on temperature, as proved in the temperature range below 2.4 K, but it strongly decreases in magnetic field. In a field of 3 Oe, τ is longer than 30 min. This behavior, different from the ac behavior, may be understood by assuming that at the moment of switching the field on, at first, individual chains quickly relax and then slow relaxations follow through nucleation and movement of domain walls (cf. Figure 7 and the corresponding text). The FC/ZFC effect and hysteresis were also observed for the previously studied compound $[Co(NCS)_2(4\text{-ethylpyridine})]_n$, but for that case, unfortunately, the temperature dependence of the relaxation time in a dc field was not determined.[53] Our present results may be compared with single-crystal results reported by Groenendijk and Duyneveldt for a canted antiferromagnet $[(CH_3)_3NH]CoCl_3{\cdot}2H_2O$; (CoTAC).[70] The fast process, which they observed in the vicinity of T_N = 4.18 K, quickly disappeared with decreasing temperature, and only one slow

dx.doi.org/10.1021/ic500572p | Inorg. Chem. 2014, 53, 8298–8310

process remained at the lowest temperatures, which was interpreted to be the domain wall process.

The absence of a thermal activation in our dc study points to the tunneling mechanism of domain relaxation. Lhotel et al. reported resonant quantum tunneling in the ferromagnetic spin chains of CoTAC.[74] This effect was observed on a single-crystal sample at very low temperatures of about 0.3 K. Wernsdorfer et al. reported quantum dynamics for a single-chain magnet composed of Mn_2Ni units below 0.7 K but without resonant effects.[75] Domain wall nucleation due to tunneling and depinning was reported to also take place at higher temperatures in mesoscopic Ni wires below 1 K[76,77] and even at 5 K.[78] Thus, the tunneling mechanism, operating in $[Co(NCS)_2(bpa)]_n$, does not seem to be impossible.

$[Co(NCS)_2(bpe)]_n$ is like a classical metamagnet. Its relaxation spectrum obtained by the ac method in zero bias field (i.e., in the antiferromagnetic phase) can be described by an assumption of only one process (Table S3) taking place in the whole studied temperature range below T_N = 4.0 K. This process is interpreted as relaxation of single chains with the activation energy Δ_τ =33.3 K. There is some distribution of the relaxation times, which is narrow at higher temperatures (α = 0.10 at 3.4 K), but considerably broadens at lower temperatures (α = 0.46 at 2.0 K). This broadening may be caused by interchain interactions. With increasing bias field above H_c the compound enters a mixed phase and the relaxation spectrum becomes more complex. We were able to resolve two processes, both related with domains, but only one of them (the faster) showed single barrier thermal activation. The activation energy Δ_τ, determined for this process, is greater than of the SCM process in the AFM phase, being 43 K in 500 Oe and decreases with increasing field. The second process seems to be a multibarrier process.

Relaxations, occurring in the mixed phase, were investigated by Baranov et al.[79] and were theoretically analyzed by Ovchinnikov et al.[80] for two Mn(II)-diradical metamagnetic chain compounds with low anisotropy. These relaxations were ascribed to nucleation and displacements of domain walls separating the antiferromagnetic and ferrimagnetic phases. It was shown that the relaxation mechanism in one of these compounds was thermally activated and engaged a single activation barrier, while in the second (with metamagnetic transition), it engaged a distribution of barriers.[80] Metamagnetic Co(II) chain systems with high anisotropy and small antiferromagnetic interchain interactions have also been reported in literature. One example is the Co(II)-radical system studied by Numata et al.[81] and analyzed by Bukharov et al.[82] This material shows relaxations in the mixed phase, which are due to nucleation and displacements of domain walls, but below 4 K, it enters into the field-induced metastable state with a wide hysteresis loop indicative of domain wall freezing.

The domain wall relaxation processes in $[Co(NCS)_2(bpa)]_n$ and $[Co(NCS)_2(bpe)]_n$ are governed by Glauber dynamics of the chains, which relax together, but in the domain wall, the antiferromagnetic interchain interactions must be overcome.[79,80] Therefore, the height of the energy barrier for these processes is enhanced. We observed the enhancement of the energy barrier for the single-barrier process in the mixed phase of $[Co(NCS)_2(bpe)]_n$. However, we were not able to observe such enhancement for $[Co(NCS)_2(bpa)]_n$, possibly because of much weaker interchain interactions.

For SCMs, the activation energy of relaxation time Δ_τ is usually discussed using the following equation

$$\Delta_\tau = k\Delta_\xi + \Delta_A \quad (8)$$

where Δ_ξ is the creation energy of the domain wall, which, by virtue of eq 2, is equal to $J/2$, k is a factor equal to 1 or 2 for finite or infinite chains, respectively, and Δ_A is the activation energy of an uncoupled anisotropic spin inside a narrow domain wall.[10] For the linear Ising system of effective spins $^1/_2$, the whole anisotropy is the exchange anisotropy; however, the real anisotropy of a single, uncoupled Co(II) ion is not infinitive but is nevertheless high. For $Co(NCS)_2(bpe)$, the value of Δ_τ/k_B (corresponding to single chains) in zero field is 33.3 K (see Table 1) and Δ_ξ/k_B = 13.0 K; thus, assuming finite chains, the anisotropy term Δ_A/k_B would be equal to 20.3 K. For $Co(NCS)_2(bpa)$, Δ_τ/k_B = 39.2 K and Δ_ξ/k_B = 14 K; thus, Δ_A/k_B = 25.2 K. The Glauber criterion $\Delta_A > \Delta_\xi$ is met for both compounds, as was expected for Ising chain systems. It is noted that an assumption of k = 2 would lead to a contradiction with the Ising model in the studied temperature range. A crossover from the finite to infinite size regime, common to SCM materials, is expected at higher temperatures.[10]

In summary, we have shown that the metamagnetic layered compounds $[Co(NCS)_2(bpa)]_n$ and $[Co(NCS)_2(bpe)]_n$, in which the ferromagnetic cobalt thiocyanato chains are linked by different bridging coligands, show different relaxation properties. When these coligands form a conjugated system like that in $[Co(NCS)_2(bpe)]_n$, the antiferromagnetic phase transition occurs due to antiferromagnetic interchain coupling. In this case, only one relaxation process is observed in zero field, whereas for the case where the interchain exchange interaction through the nonconjugated ligand is hindered, more complex relaxation behavior may appear, presumably because of other (dipolar) interchain interactions that come into play. In particular, longer relaxation times, related with domains walls, might be expected when canting between magnetic moments of interacting chains is present. Further investigations are planned for other compounds of this family, where dipolar interactions can be responsible for the interchain magnetic coupling.

EXPERIMENTAL SECTION

Chemicals. $Co(NCS)_2$ and 1,2-bis(4-pyridyl)ethane (bpa) were obtained from Alfa Aesar and Sigma-Aldrich, respectively.

Preparation of $[Co(NCS)_2(bpa)_2]_n$. $Co(NCS)_2$ (261 mg, 1.5 mmol) and 1,2-bis(4-pyridyl)ethane (520 mg, 3 mmol) were reacted in 3 mL of water at rt. After 3 days, a dark-pink crystalline powder was filtered off, washed with ethanol and diethyl ether, and dried in air. The purity was checked by XRPD and elemental analysis. Yield based on $Co(NCS)_2$: 772 mg (94.8%). Anal. Calcd for $C_{26}H_{24}CoN_6S_2$ (543.58) (%): C, 57.45; H, 4.45; N, 15.46; S, 11.80. Found: C, 57.41; H, 4.43; N, 15.45; S, 11.79.

Preparation of $[Co(NCS)_2(bpa)]_n$. $Co(NCS)_2$ (583 mg, 3.0 mmol) and 1,2-bis(4-pyridyl)-ethane (276 mg, 1.5 mmol) were reacted in 1 mL of water. After 3 days, a pink crystalline powder was filtered off, washed with ethanol and diethyl ether, and dried in air. The purity was checked by XRPD and elemental analysis. Yield based on $Co(NCS)_2$: 530 mg (98.4%). Anal. Calcd for $C_{14}H_{12}CoN_4S_2$ (359.34) (%): C, 46.80; H, 3.37; N, 15.59; S, 17.85. Found: C, 46.78; H, 3.36; N, 15.57; S, 17.83.

Elemental Analysis of the Residue in the First TG Step of the Thermal Decomposition Reaction of $[Co(NCS)_2(bpa)_2]$. Anal. Calcd for $C_{14}H_{12}CoN_4S_2$ (359.34) (%): C, 46.8; H, 3.3; N, 15.5; S, 17.8. Found: C, 47.19; H, 3.24; N, 16.31; S, 19.71. IR (ATR): ν_{max} = 2102 (s), 1610 (m), 1558 (w), 1504 (w), 1437 (w), 1423 (m), 1224 (m), 1207 (w), 1067 (m), 1016 (m), 952 (w), 932 (w), 826 (s), 789 (m), 758 (w), 548 (m), 534 (m), 520 (m), 474 (m) cm^{-1}.

dx.doi.org/10.1021/ic500572p | Inorg. Chem. 2014, 53, 8298−8310

Elemental Analysis. CHNS analysis was performed using an EURO EA elemental analyzer, produced by EURO VECTOR Instruments and Software.

Spectroscopy. All IR data were obtained using an ATI Mattson Genesis Series FTIR Spectrometer, control software: WINFIRST, from ATI Mattson.

Differential Thermal Analysis and Thermogravimetry. The DTA-TG measurements were performed in a nitrogen atmosphere (purity: 5.0) in Al_2O_3 crucibles using a STA-409CD instrument from Netzsch. All measurements were performed with a flow rate of 75 mL min^{-1} and were corrected for buoyancy and current effects. The instrument was calibrated using standard reference materials.

X-ray Powder Diffraction (XRPD). The measurements were performed using (1) a PANalytical X'Pert Pro MPD Reflection Powder Diffraction System with Cu Kα_1 radiation (λ = 1.540598 Å) equipped with a PIXcel semiconductor detector and (2) a Stoe Transmission Powder Diffraction System (STADI P) with Cu Kα_1 radiation (λ = 1.540598 Å) that was equipped with a linear position-sensitive detector from STOE & CIE.

Structure Determination from X-ray Powder Data. The powder data could be indexed with a monoclinic unit cell with a = 10.86 Å, b = 13.68 Å, c = 11.33 Å, β = 107.1°, $\alpha = \gamma$ = 90°, V = 1608 Å^3. The unit-cell volume revealed that the unit cell contains four formula units. The systematic extinctions leads to space group $P2_1/n$, with one formula unit in the asymmetric unit. A Pawley fit was used to extract the reflection intensities and their correlations. The structure was solved by real-space methods with simulated annealing using the program DASH.[83] The subsequent Rietveld refinement[84,85] was performed with the program TOPAS.[86] All atomic positions, including H atoms, were refined, but restraints were applied for the C−C, C−N, and C−H bond lengths, for C−C−C, C−C−N, C−N−C, N−C−S, and C−C−H bond angles, and for the planarity of the pyridine ring including the adjacent C and H atoms. The two pyridine rings were treated completely independent of each other; there was no assumption or restraint on the molecular conformation of the bpa ligand or on the relative orientation of the two pyridine rings. Apart from the atomic coordinates, we refined the scale factor, lattice parameters, peak profile, background, and two isotropic displacement parameters (one for Co, one for the carbon atoms). The data were slightly affected by preferred orientation, which led to a March−Dollase parameter of 1.07 in the [020] direction.[87,88] The refinements converged with good R-values and a smooth difference curve. The Rietveld plot is found in Figure S4, Supporting Information. Selected crystallographic data and details on the structure refinement are given in Table 2.

Table 2. Selected Crystallographic Data and Details on the Structure Determination from Rietveld Refinement for $[Co(NCS)_2(bpa)]_n$

formula	$C_{14}H_{12}CoN_4S_2$
MW (g mol^{-1})	359.35
crystal system	monoclinic
space group	$P2_1/n$
a (Å)	10.8555(5)
b (Å)	13.6813(5)
c (Å)	11.3271(5)
β (deg)	107.143(2)
V (Å^3)	1607.54(13)
T (K)	295
Z	4
D_{calc} (mg m^3)	1.5
λ (Å)	1.54056
μ (mm^{-1})	10.774
R_{wp}	0.1264
R_p	0.0974
GOF	1.308

CCDC ($[Co(NCS)_2(bpa)]_n$) contain the supplementary crystallographic data for this paper. These data can be obtained free charge from the Cambridge Crystallographic Data Centre via http://www.ccdc.cam.ac.uk/data_request/cif.

Magnetic Measurements. Magnetic measurements were performed on powder samples using a PPMS (Physical Property Measurement System) from Quantum Design, which was equipped with a 9 T superconducting magnet. Some measurements were also performed with a Quantum Design SQUID magnetometer, model XPMS-5XL and with a LakeShore ac-susceptometer/dc-magnetometer, model 7225. In the field-cooling regime (FC), the sample was cooled in a specific field; next, its magnetization was measured in this field on heating. In the zero-field cooling (ZFC) regime, the sample was cooled in zero field; next, its magnetization was measured in this field on heating. ac measurements were done with the amplitude of ac driving field of 3 or 5 Oe. The samples were strongly hand-pressed and, for some measurements, frozen in Nujol. The data were corrected for the diamagnetism using the tabulated Pascal's constants.

■ ASSOCIATED CONTENT

Ⓢ Supporting Information

XRPD pattern, IR spectra, and additional magnetic data. This material is available free of charge via the Internet at http://pubs.acs.org.

■ AUTHOR INFORMATION

Corresponding Author

*Fax: +49 431-880 1520; Tel: +49 431-880 1520; E-mail: cnaether@ac.uni-kiel.de.

Notes

The authors declare no competing financial interest.

■ ACKNOWLEDGMENTS

This project was supported by the Deutsche Forschungsgemeinschaft (project no. Na 720/5-1) and the State of Schleswig-Holstein. We thank Prof. Dr. Wolfgang Bensch for access to his experimental facilities. Special thanks to Henning Lühmann and Maren Rasmussen for performing several magnetic measurements.

■ REFERENCES

(1) Caneschi, A.; Gatteschi, D.; Lalioti, N.; Sangregorio, C.; Sessoli, R.; Venturi, G.; Vindigni, A.; Rettori, A.; Pini, M. G.; Novak, M. A. *Angew. Chem., Int. Ed.* **2001**, *40*, 1760−1763.

(2) Sun, H. L.; Wang, Z. M.; Gao, S. *Coord. Chem. Rev.* **2010**, *254*, 1081−1100.

(3) Miyasaka, H.; Clérac, R. *Bull. Chem. Soc. Jpn.* **2005**, *78*, 1725−1748.

(4) Pardo, E.; Train, C.; Lescouezec, R.; Journaux, Y.; Pasan, J.; Ruiz-Perez, C.; Delgado, F. S.; Ruiz-Garcia, R.; Lloret, F.; Paulsen, C. *Chem. Commun.* **2010**, *46*, 2322−2324.

(5) Yang, C.-I.; Hung, S.-P.; Lee, G.-H.; Nakano, M.; Tsai, H.-L. *Inorg. Chem.* **2010**, *49*, 7617−7619.

(6) Zhao, J.-P.; Yang, Q.; Liu, Z.-Y.; Zhao, R.; Hu, B.-W.; Du, M.; Chang, Z.; Bu, X.-H. *Chem. Commun.* **2012**, *48*, 6568−6570.

(7) Ouellette, W.; Prosvirin, A. V.; Whitenack, K.; Dunbar, K. R.; Zubieta, J. *Angew. Chem., Int. Ed.* **2009**, *48*, 2140−2143.

(8) Prosvirin, A. V.; Zhao, H.; Dunbar, K. R. *Inorg. Chim. Acta* **2012**, *389*, 118−121.

(9) Feng, X.; Liu, J.; Harris, T. D.; Hill, S.; Long, J. R. *J. Am. Chem. Soc.* **2012**, *134*, 7521−7529.

(10) Coulon, C.; Miyasaka, H.; Clérac, R. *Struct. Bonding (Berlin, Ger.)* **2006**, *122*, 163−206.

(11) Bernot, K.; Luzon, J.; Sessoli, R.; Vindigni, A.; Thion, J.; Richeter, S.; Leclercq, D.; Larionova, J.; van der Lee, A. *J. Am. Chem. Soc.* **2008**, *130*, 1619−1627.

(12) Bałanda, M.; Rams, M.; Nayak, S. K.; Tomkowicz, Z.; Haase, W.; Tomala, K.; Yakhmi, J. V. *Phys. Rev. B* **2006**, *74*, 224421.
(13) Bałanda, M.; Tomkowicz, Z.; Haase, W.; Rams, M. *J. Phys.: Conf. Ser.* **2010**, *303*, 012036.
(14) Cariati, E.; Ugo, R.; Santoro, G.; Tordin, E.; Sorace, L.; Caneschi, A.; Sironi, A.; Macchi, P.; Casati, N. *Inorg. Chem.* **2010**, *49*, 10894−10901.
(15) Coronado, E.; Galan-Mascarós, J. R.; Martí-Gastaldo, C. *J. Am. Chem. Soc.* **2008**, *130*, 14987−14989.
(16) Ferbinteanu, M.; Miyasaka, H.; Wernsdorfer, W.; Nakata, K.; Sugiura, K.-i.; Yamashita, M.; Coulon, C.; Clérac, R. *J. Am. Chem. Soc.* **2005**, *127*, 3090−3099.
(17) Ferrando-Soria, J.; Pardo, E.; Ruiz-García, R.; Cano, J.; Lloret, F.; Julve, M.; Journaux, Y.; Pasán, J.; Ruiz-Pérez, C. *Chem.—Eur. J.* **2011**, *17*, 2176−2188.
(18) Kajiwara, T.; Nakano, M.; Kaneko, Y.; Takaishi, S.; Ito, T.; Yamashita, M.; Igashira-Kamiyama, A.; Nojiri, H.; Ono, Y.; Kojima, N. *J. Am. Chem. Soc.* **2005**, *127*, 10150−10151.
(19) Kajiwara, T.; Tanaka, H.; Nakano, M.; Takaishi, S.; Nakazawa, Y.; Yamashita, M. *Inorg. Chem.* **2010**, *49*, 8358−8370.
(20) Mitsumoto, K.; Ui, M.; Nihei, M.; Nishikawa, H.; Oshio, H. *CrystEngComm* **2010**, *12*, 2697−2699.
(21) Stamatatos, T. C.; Abboud, K. A.; Wernsdorfer, W.; Christou, G. *Inorg. Chem.* **2009**, *48*, 807−809.
(22) Yang, C.-I.; Chuang, P.-H.; Lu, K.-L. *Chem. Commun.* **2011**, *47*, 4445−4447.
(23) Bhargavi, G.; Rajasekharan, M. V.; Costes, J. P.; Tuchagues, J. P. *Dalton Trans.* **2013**, *42*, 8113−8123.
(24) Dong, D.-P.; Zhang, Y.-J.; Zheng, H.; Zhuang, P.-F.; Zhao, L.; Xu, Y.; Hu, J.; Liu, T.; Duan, C.-Y. *Dalton Trans.* **2013**, *42*, 7693−7698.
(25) Li, X.-B.; Zhuang, G.-M.; Wang, X.; Wang, K.; Gao, E.-Q. *Chem. Commun.* **2013**, *49*, 1814−1816.
(26) Liu, T.; Zheng, H.; Kang, S.; Shiota, Y.; Hayami, S.; Mito, M.; Sato, O.; Yoshizawa, K.; Kanegawa, S.; Duan, C. *Nat. Commun.* **2013**, *4*, 2826.
(27) Tangoulis, V.; Lalia-Kantouri, M.; Gdaniec, M.; Papadopoulos, C.; Miletic, V.; Czapik, A. *Inorg. Chem.* **2013**, *52*, 6559−6569.
(28) Miyasaka, H.; Madanbashi, T.; Saitoh, A.; Motokawa, N.; Ishikawa, R.; Yamashita, M.; Bahr, S.; Wernsdorfer, W.; Clérac, R. *Chem.—Eur. J.* **2012**, *18*, 3942−3954.
(29) Bhowmick, I.; Hillard, E. A.; Dechambenoit, P.; Coulon, C.; Harris, T. D.; Clerac, R. *Chem. Commun.* **2012**, *48*, 9717−9719.
(30) Harris, T. D.; Bennett, M. V.; Clérac, R.; Long, J. R. *J. Am. Chem. Soc.* **2010**, *132*, 3980−3988.
(31) Coulon, C.; Clérac, R.; Wernsdorfer, W.; Colin, T.; Miyasaka, H. *Phys. Rev. Lett.* **2009**, *102*, 164204−164207.
(32) Näther, C.; Greve, J. *J. Solid State Chem.* **2003**, *176*, 259−265.
(33) Wriedt, M.; Sellmer, S.; Näther, C. *Inorg. Chem.* **2009**, *48*, 6896−6903.
(34) Wriedt, M.; Sellmer, S.; Näther, C. *Dalton Trans.* **2009**, 7975−7984.
(35) Wriedt, M.; Jeß, I.; Näther, C. *Eur. J. Inorg. Chem.* **2009**, 1406−1413.
(36) Wriedt, M.; Näther, C. *Chem. Commun.* **2010**, *46*, 4707−4709.
(37) Näther, C.; Wöhlert, S.; Boeckmann, J.; Wriedt, M.; Jeß, I. *Z. Anorg. Allg. Chem.* **2013**, *639*, 2696−2714.
(38) Zurowska, B.; Mrozinski, J.; Julve, M.; Lloret, F.; Maslejova, A.; Sawka-Dobrowolska, W. *Inorg. Chem.* **2002**, *41*, 1771−1777.
(39) Shurdha, E.; Lapidus, S. H.; Stephens, P. W.; Moore, C. E.; Rheingold, A. L.; Miller, J. S. *Inorg. Chem.* **2012**, *51*, 9655−9665.
(40) Machura, B.; Świtlicka, A.; Zwoliński, P.; Mroziński, J.; Kalińska, B.; Kruszynski, R. *J. Solid State Chem.* **2013**, *197*, 218−227.
(41) Machura, B.; Świtlicka, A.; Mroziński, J.; Kalińska, B.; Kruszynski, R. *Polyhedron* **2013**, *52*, 1276−1286.
(42) Machura, B.; Palion, J.; Penkala, M.; Groń, T.; Duda, H.; Kruszynski, R. *Polyhedron* **2013**, *56*, 189−199.
(43) Małecki, J. G.; Groń, T.; Duda, H. *Polyhedron* **2012**, *36*, 56−68.
(44) González, R.; Acosta, A.; Chiozzone, R.; Kremer, C.; Armentano, D.; De Munno, G.; Julve, M.; Lloret, F.; Faus, J. *Inorg. Chem.* **2012**, *51*, 5737−5747.
(45) Machura, B.; Świtlicka, A.; Nawrot, I.; Mroziński, J.; Kruszynski, R. *Polyhedron* **2011**, *30*, 832−840.
(46) Ma, Q.; Zhu, M.; Lu, L.; Feng, S.; Yan, J. *Inorg. Chim. Acta* **2011**, *370*, 102−107.
(47) Bhowmik, P.; Chattopadhyay, S.; Drew, M. G. B.; Diaz, C.; Ghosh, A. *Polyhedron* **2010**, *29*, 2637−2642.
(48) Barasiński, A.; Sobczak, P.; Drzewiński, A.; Kamieniarz, G.; Bieńko, A.; Mroziński, J.; Gatteschi, D. *Polyhedron* **2010**, *29*, 1485−1491.
(49) Boeckmann, J.; Näther, C. *Dalton Trans.* **2010**, *39*, 11019−11026.
(50) Boeckmann, J.; Näther, C. *Chem. Commun.* **2011**, *47*, 7104−7106.
(51) Foner, S.; Frankel, R. B.; Reiff, W. M.; Little, B. F.; Long, G. J. *Solid State Commun.* **1975**, *16*, 159−161.
(52) Boeckmann, J.; Wriedt, M.; Näther, C. *Chem.—Eur. J.* **2012**, *18*, 5284−5289.
(53) Wöhlert, S.; Fic, T.; Tomkowicz, Z.; Ebbinghaus, S. G.; Rams, M.; Haase, W.; Näther, C. *Inorg. Chem.* **2013**, *52*, 12947−12957.
(54) Zhang, S.-Y.; Shi, W.; Lan, Y.; Xu, N.; Zhao, X.-Q.; Powell, A. K.; Zhao, B.; Cheng, P.; Liao, D.-Z.; Yan, S.-P. *Chem. Commun.* **2011**, *47*, 2859−2861.
(55) Zhang, X.-M.; Wang, Y.-Q.; Wang, K.; Gao, E.-Q.; Liu, C.-M. *Chem. Commun.* **2011**, *47*, 1815−1817.
(56) Wöhlert, S.; Boeckmann, J.; Wriedt, M.; Näther, C. *Angew. Chem., Int. Ed.* **2011**, *50*, 6920−6923.
(57) Wöhlert, S.; Ruschewitz, U.; Näther, C. *Cryst. Growth Des.* **2012**, *12*, 2715−2718.
(58) Wöhlert, S.; Wriedt, M.; Fic, T.; Tomkowicz, Z.; Haase, W.; Näther, C. *Inorg. Chem.* **2013**, *52*, 1061−1068.
(59) Allen, F. *Acta Crystallogr.* **2002**, *B58*, 380−388.
(60) Hernandez, M. L.; Gotzone Barandika, M.; Karmele Urtiaga, M.; Cortes, R.; Lezama, L.; Isabel Arriortua, M.; Rojo, T. *J. Chem. Soc., Dalton Trans.* **1999**, 1401−1406.
(61) Merz, C.; Desciak, M.; O'Brien, C.; LaDuca, R. L.; Finn, R. C.; Rarig, R. S.; Zubieta, J. A. *Inorg. Chim. Acta* **2004**, *357*, 3331−3335.
(62) Frank, C. W.; Rogers, L. B. *Inorg. Chem.* **1966**, *5*, 615−622.
(63) Van Albada, G. A.; De Graaff, R. A. G.; Haasnoot, J. G.; Reedijk, J. *Inorg. Chem.* **1984**, *23*, 1404−1408.
(64) Kahn, O. *Molecular Magnetism*; Wiley VCH, New York, 1993.
(65) Fisher, M. E. *J. Math. Phys.* **1963**, *4*, 124−135.
(66) Etzkorn, S. J.; Hibbs, W.; Miller, J. S.; Epstein, A. J. *Phys. Rev. B* **2004**, *70*, 134419.
(67) Gatteschi, D.; Sessoli, R.; Villain, J. *Molecular Nanomagnets*; Oxford University Press: New York, 2006.
(68) Pini, M. G.; Rettori, A.; Bogani, L.; Lascialfari, A.; Mariani, M.; Caneschi, A.; Sessoli, R. *Phys. Rev. B* **2011**, *84*, 094444.
(69) Miyasaka, H.; Takayama, K.; Saitoh, A.; Furukawa, S.; Yamashita, M.; Clérac, R. *Chem.—Eur. J.* **2010**, *16*, 3656−3662.
(70) Groenendijk, H. A.; Van Duyneveldt, A. J. *Physica* **1982**, *115B*, 41−62.
(71) Carlin, R. L.; van Duyneveldt, A. J. *Acc. Chem. Res.* **1980**, *13*, 231−236.
(72) Hoogerbeets, R.; Wiegers, S. A. J.; van Duyneveldt, A. J.; Willett, R. D.; Geiser, U. *Physica B* **1984**, *125*, 135−149.
(73) van Duyneveldt, A. J. *J. Appl. Phys.* **1982**, *53*, 8006−8011.
(74) Lhotel, E.; Khatsko, E. N.; Paulsen, C. *Phys. Rev. B* **2006**, *74*, 020402(R).
(75) Wernsdorfer, W.; Clérac, R.; Coulon, C.; Lecren, L.; Miyasaka, H. *Phys. Rev. Lett.* **2005**, *95*, 237203.
(76) Wernsdorfer, W.; Doudin, B.; Mailly, D.; Hasselbach, K.; Benoit, A.; Meier, J.; Ansermet, J. P.; Barbara, B. *Phys. Rev. Lett.* **1996**, *77*, 1873−1876.
(77) Wernsdorfer, W.; Hasselbach, K.; Benoit, A.; Barbara, B.; Doudin, B.; Meier, J.; Ansermet, J. P.; Mailly, D. *Phys. Rev. B* **1997**, *55*, 11552−11559.

(78) Hong, K.; Giordano, N. *Europhys. Lett.* **1996**, *36*, 147−152.
(79) Baranov, N. V.; Mushnikov, N. V.; Goto, T.; Hosokoshi, Y.; Inoue, K. *J. Phys.: Condens. Matter* **2003**, *15*, 8881.
(80) Ovchinnikov, A. S.; Bostrem, I. G.; Sinitsyn, V. E.; Boyarchenkov, A. S.; Baranov, N. V.; Inoue, K. *Phys. Rev. B* **2006**, *74*, 174427.
(81) Numata, Y.; Inoue, K.; Baranov, N.; Kurmoo, M.; Kikuchi, K. *J. Am. Chem. Soc.* **2007**, *129*, 9902−9909.
(82) Bukharov, A. A.; Ovchinnikov, A. S.; Baranov, A. V.; Inoue, K. *J. Phys.: Condens. Matter* **2010**, *22*, 436003 .
(83) David, W. I. F.; Shankland, K.; Van de Streek, J.; Pidcock, E.; Motherwell, S. *J. Appl. Crystallogr.* **2006**, *39*, 910−915.
(84) Rietveld, H. *Acta Crystallogr.* **1967**, *22*, 151−152.
(85) Rietveld, H. M. *J. Appl. Crystallogr.* **1969**, *2*, 65−71.
(86) Coelho, A. A. *TOPAS*; Coelho Software: Brisbane, Australia, 2007.
(87) Dollase, W. *J. Appl. Crystallogr.* **1986**, *19*, 267−272.
(88) March, A. *Z. Kristallogr.* **1932**, *81*, 285−297.